

# Coherent-feedback formulation of a continuous quantum error correction protocol

Joseph Kerckhoff,<sup>1</sup> Hendra I. Nurdin,<sup>1,2</sup> Dmitri S. Pavlichin,<sup>1</sup> and Hideo Mabuchi<sup>1</sup>

<sup>1</sup>*Edward L. Ginzton Laboratory, Stanford University, Stanford, California 94305, USA*

<sup>2</sup>*Department of Information Engineering, The Australian National University, Canberra, ACT 0200, Australia*

(Dated: August 28, 2009)

We propose an approach to quantum error correction based on coding and continuous syndrome readout via scattering of coherent probe fields, in which the usual steps of measurement and discrete restoration are replaced by unitary processing of the probe beams and coherent feedback to the register qubits. We exploit a limit theorem for quantum stochastic differential equations to analyze coherent feedback networks based on the bit-flip/phase-flip code, obtaining simple closed-loop master equations with only four Hilbert-space dimensions required for the controller. Our approach is well matched to physical implementations that feature solid-state qubits embedded in planar electromagnetic circuits.

PACS numbers: 03.67.Pp, 02.30.Yy, 42.50.-p, 03.65.Yz

Fundamental concepts of quantum error correction (QEC) based on coding and measurement of syndromes [1] have become central to the modern field of quantum information science. Although substantial work is still being devoted to extensions and refinements of abstract QEC theory, some efforts [2–4] have begun to focus on the complementary task of developing implementation approaches that apply the fundamental principles of QEC in ways that naturally accommodate the structure of elementary physical models. Such new approaches could enable the design of quantum memories that make more efficient use of critical physical resources and introduce new physically-motivated abstractions for quantum circuit engineering to complement those we have inherited from classical computer science.

Working in this spirit, we recently proposed [5] a cavity quantum electrodynamics (cavity QED) implementation of the homodyne-type parity measurement required for a continuous-QEC [6–12] version of the familiar three-qubit bit-flip or phase-flip codes, which becomes very simple to model in a strong coupling limit. In this article we take the further step of describing coherent feedback networks that realize quantum memories in which decoherence of the encoded qubit is suppressed without the need for any measurement-based filtering or feedback. Our results establish an important new link between quantum information science and the nascent theory of coherent-feedback quantum control [13–16], and highlight the possibility of incorporating ‘embedded controllers’ in quantum information processing platforms based on optical or microwave resonator/waveguide circuits [17–19]. The modeling framework that we utilize, based on quantum stochastic differential equations (QSDE’s), is sufficiently general to allow the incorporation of signal fields that carry information simultaneously in non-commuting quadratures. While this is not strictly necessary for the type of scheme we consider here, which simply allocates one probe field per stabilizer generator, it is possible that future work in this setting could ex-

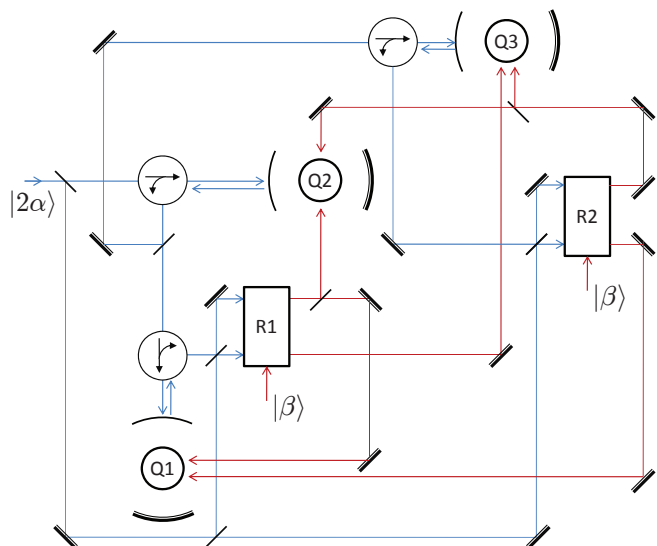


FIG. 1: Schematic diagram of a coherent-feedback quantum memory showing qubits-in-cavities (Q1, Q2 and Q3), circulators, beam-splitters, steering mirrors and relays (R1 and R2). The calculation we present is based on a modified arrangement that leads to the same closed-loop master equation but factorizes into four simple sub-networks.

plore more general quantum memory architectures with reduced resource overhead.

We begin the presentation of our approach with the schematic diagram shown in Fig. 1. For a memory based on the bit-flip or phase-flip code, three register qubits (Q1, Q2 and Q3) are required and we assume that each is strongly coupled to its own electromagnetic resonator (cavity). Two probe beams and two reference beams are generated from a coherent input  $|2\alpha\rangle$  (where  $|\alpha|^2$  has units photons  $\text{time}^{-1}$ ); the probe beams scatter (reflect) from the cavities as shown in the diagram. As described in [5] the beam that scatters from qubit-cavities Q2 and Q1 carries a coherent amplitude  $\alpha Z_1 Z_2$ , where  $Z_i$  is the Pauli  $\sigma_z$  operator on qubit  $i$ , and when it is

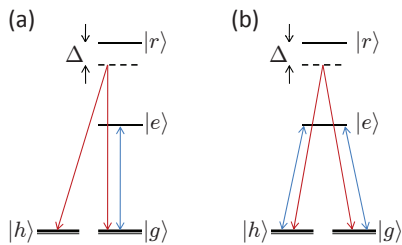


FIG. 2: Level diagrams for pre-limit models of (a)  $Z$  probe interaction, (b)  $X$  probe interaction.

recombined with one of the reference beams at a beam-splitter the two output ports carry coherent amplitudes  $\alpha(1 \pm Z_1 Z_2)/\sqrt{2}$ . These two signals are used as set and reset inputs to a flip-flop relay (see below) that controls the routing of a coherent beam with amplitude  $\beta$  and a distinct frequency from that of the probe beams, sending it either directly to Q3 or to a beam-splitter that evenly divides its power between Q1 and Q2. Similarly, the other probe and reference beam generate  $\alpha(1 \pm Z_3 Z_2)/\sqrt{2}$ , which are used as inputs to a relay that controls the routing of another frequency-shifted beam with amplitude  $\beta$ , sending it either directly to Q1 or splitting its power between Q2 and Q3. As a result the illumination conditions for driving a Raman transition are completed on at most one qubit, depending on the values of the syndrome generators  $Z_1 Z_2$  and  $Z_3 Z_2$  (below we will discuss an additional mechanism for compensation of ac Stark shifts). This feedback protocol turns on a corrective bit-flipping Hamiltonian for any qubit that the probes indicate as having experienced an error.

This coherent feedback network thus implements a continuous version of the usual discrete-step strategy. In our scheme  $\alpha$  and  $\beta$  take the place of the discrete design parameter  $\tau$ , the time interval between executions of the circuit that implements syndrome measurement and unitary restoration. Note that clocked execution of a special measurement/restoration circuit is not required in our approach—with the physical component models described below, the operation of the coherent controller is *stationary* in the sense that  $\alpha$ ,  $\beta$ , and all Hamiltonian coupling constants are constant in time. Other than the coherent field inputs no interfacing to external detectors or electronics is required for our scheme. As long as the relays can be implemented in the same hardware platform as the register qubits, the coherent controller can be entirely ‘on-chip.’ In this sense it is roughly analogous to the impedance network in a feedback loop around an electronic operational amplifier, which tunes and stabilizes its frequency response, or to the dynamic mechanical components utilized in James Watt’s flyball governor.

Although we have referred to Q1, Q2 and Q3 thus far as qubits, we actually need to utilize a multi-level internal structure to facilitate both the probe interactions and the Raman (corrective) bit-flips. Fig. 2(a) shows the level

structure required for a bit-flip memory, and Fig. 2(b) for a phase-flip memory. In the bit-flip implementation, we assume that each qubit is strongly coupled to a single-mode, single-sided cavity on its  $|g\rangle \leftrightarrow |e\rangle$  transition as discussed in [5]. As a result, the phase acquired on reflection by a probe beam is 0 if the qubit is in state  $|g\rangle$  and  $\pi$  if it is in  $|h\rangle$ . While details of the probe-qubit interaction can be investigated for any desired physical parameters using the familiar cavity QED master equation, for our network calculation we will utilize a simple abstraction obtained as the vacuum Rabi frequency  $g_p$  and cavity field decay rate  $\kappa_p$  are taken to infinity (strong coupling limit) with  $g_p/\kappa_p$  fixed. The simplified model is derived using a QSDE limit theorem [20] following a similar procedure to that of [5]. In the phase-flip scenario we modify the scheme by assuming a linearly polarized cavity mode (as in a micro-disk or photonic crystal resonator) that couples to both a  $\sigma_-$  transition from  $|g\rangle \leftrightarrow |e\rangle$  and a  $\sigma_+$  transition from  $|h\rangle \leftrightarrow |e\rangle$ .

For use below we define the resulting bit-flip probe interaction models  $Q_{13} = (Z_1, 0, 0)$ ,  $Q_{21} = Q_{24} = (Z_2, 0, 0)$ ,  $Q_{31} = (Z_3, 0, 0)$  (modifications for the phase-flip scenario will be discussed in conjunction with the full closed-loop master equation). Here we are summarizing quantum input-output models in terms of the  $(S, L, H)$  coefficients for the evolution of a QSDE right-propagator [21]. A summary of the QSDE formalism is beyond our present scope, but to provide some intuition we note that the  $(S, L, H)$  coefficients play a similar role in the theory of open quantum systems to that of S-parameters in electrical circuit design. For the Raman transitions,

$$\begin{aligned} S^{(Q_{11})} &= 1, & L^{(Q_{11})} &= \sqrt{\gamma} \left( \sigma_{gr}^{(Q_1)} + \sigma_{gG}^{(Q_1)} \right), \\ H^{(Q_{11})} &= \Delta \left( \frac{1}{2} \Pi_r^{(Q_1)} - \Pi_G^{(Q_1)} \right), \\ S^{(Q_{12})} &= 1, & L^{(Q_{12})} &= \sqrt{\gamma} \left( \sigma_{hr}^{(Q_1)} + \sigma_{hH}^{(Q_1)} \right), \\ H^{(Q_{12})} &= \Delta \left( \frac{1}{2} \Pi_r^{(Q_1)} - \Pi_H^{(Q_1)} \right), \end{aligned}$$

and  $(S, L, H)$  for  $Q_{22}$  and  $Q_{32}$  correspond to those of  $Q_{11}$  with all operators on  $Q_1$  replaced by operators on  $Q_2$  and  $Q_3$ , respectively;  $(S, L, H)$  for  $Q_{23}$  and  $Q_{33}$  correspond to those of  $Q_{12}$  with all operators on  $Q_1$  replaced by operators on  $Q_2$  and  $Q_3$ , respectively. Here  $\Pi_k^{(C)}$  and  $\sigma_{jk}^{(C)}$  represent  $|k\rangle\langle k|$  and  $|j\rangle\langle k|$  on the Hilbert space of component  $C$ . Note that we have included two extra qubit levels  $|G\rangle$  and  $|H\rangle$  with equal but opposite detuning to that of  $|r\rangle$ , plus extra coupling terms between  $|g\rangle \leftrightarrow |G\rangle$ , driven only by one of the Raman beams, and  $|h\rangle \leftrightarrow |H\rangle$ , driven only by the other. The purpose of these terms is to compensate for ac Stark shifts that occur in our scheme. Here we have added couplings of the (theoretically) simplest possible form to accomplish such compensation, which require a somewhat awkward level scheme,

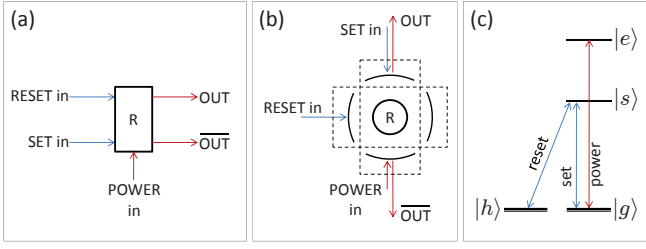


FIG. 3: Details of the ‘set-reset flip-flop cross-over relay’ component model [22]: (a) input and output ports, (b) coupling of input/output fields to resonant modes of two cavities, and (c) relay internal level diagram.

but in a practical implementation it would be possible to utilize double-pole double-throw relays that switch not only the Raman beam itself but also an auxiliary beam whose frequency, polarization and amplitude is chosen so that it provides equivalent compensation.

Some details of our relay model are displayed in Fig. 3 [22]. In electrical engineering parlance, the devices we utilize correspond to open quantum systems versions of a cross-over relay driven by a set-reset flip-flop. Each relay  $R_k$  has an internal state in the span of  $\{|g_{(R_k)}\rangle, |h_{(R_k)}\rangle\}$ . When  $R_k$  is in state  $|h_{(R_k)}\rangle$  its power input is connected to the OUT output port; when  $R_k$  is in state  $|g_{(R_k)}\rangle$  its power input is connected to the  $\overline{\text{OUT}}$  port. A probe signal driving the SET input port (in the absence of signal at the RESET input) causes the relay state to decay to  $|h\rangle$ , while driving only the RESET input induces decay to  $|g\rangle$ . Starting from a pre-limit cavity QED model in which transitions among relay states are coupled via the usual Jaynes-Cummings interaction to cavity modes, which are in turn driven by the relay input fields as shown in Fig. 3(b,c), we perform an adiabatic elimination of the excited states  $\{|e\rangle, |s\rangle\}$  using the limit theorem of [20] to arrive at the following simplified component models for relays  $R_1$  and  $R_2$ :

$$S^{(R_{k1})} = \begin{bmatrix} \Pi_g^{(R_k)} & -\Pi_h^{(R_k)} \\ -\Pi_h^{(R_k)} & \Pi_g^{(R_k)} \end{bmatrix}, \quad L^{(R_{k1})} = \begin{bmatrix} \beta \Pi_g^{(R_k)} \\ -\beta \Pi_h^{(R_k)} \end{bmatrix},$$

$$S^{(R_{k2})} = \begin{bmatrix} \Pi_h^{(R_k)} & -\sigma_{hg}^{(R_k)} \\ -\sigma_{gh}^{(R_k)} & \Pi_g^{(R_k)} \end{bmatrix}, \quad L^{(R_{k2})} = 0,$$

and  $H^{(R_{k1})} = H^{(R_{k2})} = 0$ . For the strong coupling limit we have again taken  $g_{P,s,r}, \kappa_{P,s,r} \rightarrow \infty$  with  $g_P/\kappa_P$  fixed for the POWER cavity mode and  $g_{s,r}^2/\kappa_{s,r}$  fixed for the SET and RESET cavity modes.

In addition to the above qubit and relay models, we will utilize the following component models for beam-splitters:

$$B_k : \left( \begin{bmatrix} \frac{1}{\sqrt{2}} & -\frac{1}{\sqrt{2}} \\ \frac{1}{\sqrt{2}} & \frac{1}{\sqrt{2}} \end{bmatrix}, \begin{bmatrix} \alpha_k \\ \alpha_k \end{bmatrix}, 0 \right),$$

with  $\alpha_k = \alpha$  for  $k \in \{1, 2\}$  and zero otherwise. Having now defined all the necessary component models,

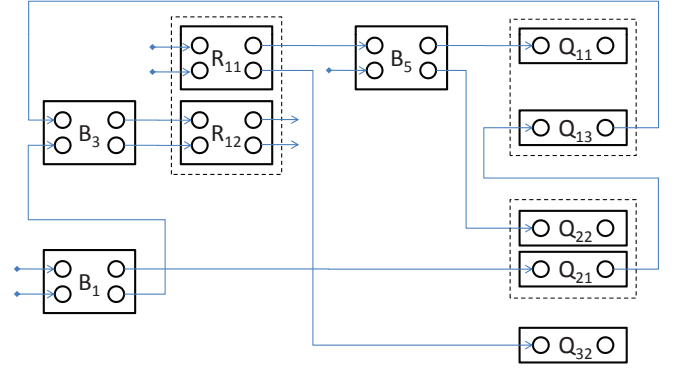


FIG. 4: Signal-flow diagram of the half-network  $G_p \boxplus G_f$ .

we proceed to assemble the full network model  $N = G_p \boxplus G_f \boxplus G'_p \boxplus G'_f \boxplus G_\Gamma$ . Here  $G_\Gamma = (\sqrt{\Gamma}X_1, 0, 0) \boxplus (\sqrt{\Gamma}X_2, 0, 0) \boxplus (\sqrt{\Gamma}X_3, 0, 0)$  describes bit-flip decoherence of the register qubits, and the component connections for  $G_p \boxplus G_f$  are shown in Fig. 4 (note that as the signal routing shown in Fig. 1 yields rather unwieldy network calculations, we are here adopting a modified routing that leads to the same closed-loop master equation with less work). Components  $\{B_1, B_3, B_5\}$  represent beam-splitters,  $\{R_{11}, R_{12}\}$  jointly represent a set-reset flip-flop relay,  $\{Q_{13}, Q_{21}\}$  are probe interactions, and  $\{Q_{11}, Q_{22}, Q_{32}\}$  are Raman interactions. Using the series  $\triangleleft$  and concatenation  $\boxplus$  products for QSDE’s [21] (where  $\boxplus_m$  represents concatenation followed by a permutation of the field mode indices such that the modes of the system to the right of  $\boxplus_m$  are inserted between the  $(m-1)^{th}$  and  $m^{th}$  modes of the left system), we define

$$G_p = R_{12} \triangleleft B_3 \triangleleft ((Q_{13} \triangleleft Q_{21}) \boxplus (1, 0, 0)) \triangleleft B_1,$$

$$G_f = (Q_{11} \boxplus Q_{32} \boxplus Q_{22}) \triangleleft (B_5 \boxplus (1, 0, 0))$$

$$\triangleleft (R_{11} \boxplus (1, 0, 0)). \quad (1)$$

Here  $G_p$  represents the ‘probe’ signal path while  $G_f$  represents the ‘feedback’ signal path; despite the fact that the QSDE coefficients of these two paths can be computed separately, a true feedback *loop* is created by the signal connection from  $Q_{13}$  to  $B_3$  because  $R_{11}$  and  $R_{12}$  act on a common Hilbert space (the state of the relay). The models for  $G'_p$  and  $G'_f$  are finally obtained from  $G_p$  and  $G_f$  by the substitutions  $B_1 \mapsto B_2$ ,  $B_3 \mapsto B_4$ ,  $R_{12} \mapsto R_{22}$ ,  $R_{11} \mapsto R_{21}$ ,  $B_5 \mapsto B_6$ ,  $Q_{11} \mapsto Q_{23}$ ,  $Q_{22} \mapsto Q_{33}$ ,  $Q_{32} \mapsto Q_{12}$ ,  $Q_{21} \mapsto Q_{24}$ ,  $Q_{13} \mapsto Q_{31}$ .

After inserting the bit-flip component models described above and applying an adiabatic elimination of the qubit excited states  $|r\rangle$ ,  $|G\rangle$  and  $|H\rangle$  (using the limit theorem of [20] with  $\beta, \Delta \rightarrow \infty$  with  $\beta^2/\Delta$  fixed), we obtain the closed-loop master equation

$$\dot{\rho}_t = -i[H, \rho_t] + \sum_{i=1}^7 \left( L_i \rho_t L_i^* - \frac{1}{2} \{L_i^* L_i, \rho_t\} \right), \quad (2)$$

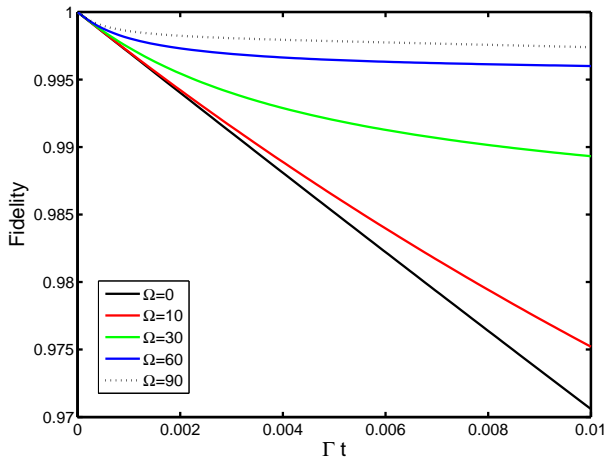


FIG. 5: Decay of fidelity,  $\langle \Psi_0 | \rho_t | \Psi_0 \rangle$ , for  $\alpha = 10$ ,  $\Gamma = 0.01$  and several values of the feedback parameter  $\Omega = \beta^2 / \gamma \Delta$ .

where ( $\Omega \equiv \beta^2 / \gamma \Delta$ )

$$\begin{aligned}
 H &= \sqrt{2}\Omega \Pi_g^{(R_1)} \Pi_h^{(R_2)} X_1 + \sqrt{2}\Omega \Pi_h^{(R_1)} \Pi_g^{(R_2)} X_3 \\
 &\quad - \Omega \Pi_g^{(R_1)} \Pi_g^{(R_2)} X_2, \\
 L_1 &= \frac{\alpha}{\sqrt{2}} \left\{ \sigma_{hg}^{(R_1)} (1 + Z_1 Z_2) + \Pi_h^{(R_1)} (1 - Z_1 Z_2) \right\}, \\
 L_2 &= \frac{\alpha}{\sqrt{2}} \left\{ \sigma_{gh}^{(R_1)} (1 - Z_1 Z_2) + \Pi_g^{(R_1)} (1 + Z_1 Z_2) \right\}, \\
 L_3 &= \frac{\alpha}{\sqrt{2}} \left\{ \sigma_{hg}^{(R_2)} (1 + Z_3 Z_2) + \Pi_h^{(R_2)} (1 - Z_3 Z_2) \right\}, \\
 L_4 &= \frac{\alpha}{\sqrt{2}} \left\{ \sigma_{gh}^{(R_2)} (1 - Z_3 Z_2) + \Pi_g^{(R_2)} (1 + Z_3 Z_2) \right\}, \\
 L_5 &= \sqrt{\Gamma} X_1, \quad L_6 = \sqrt{\Gamma} X_2, \quad L_7 = \sqrt{\Gamma} X_3. \quad (3)
 \end{aligned}$$

Note that several  $L_i$  terms corresponding to strong dephasing of the relay states have been omitted as they have no effect on the dynamics. An analogous procedure using the phase-flip component models leads to a master equation with the substitutions  $Z_i \leftrightarrow X_i$ , and indeed from the general structure of Eq. (3) it is straightforward to intuit master equations that correspond abstractly to memories based on other stabilizer codes.

In Fig. 5 we display some illustrative numerical integrations [23] of Eq. (2) for the bit-flip scenario. With the flip rate set to  $\Gamma = 0.01$  (per qubit) and the probe amplitude fixed at  $\alpha = 10$ , the feedback amplitude is varied from  $\Omega = 0$  (no feedback) to  $\Omega = 90$ . The initial state of the qubit register is chosen as  $|\Psi_0\rangle = (|ggg\rangle - i|hhh\rangle) / \sqrt{2}$ ,  $\rho_0 = |\Psi_0\rangle\langle\Psi_0|$ , and the fidelity decay  $\langle \Psi_0 | \rho_t | \Psi_0 \rangle$  is computed to quantify the decoherence suppression achieved by the coherent feedback loop. With  $\Omega = 0$  the fidelity decay is identical to that of the three-qubit register without any measurement or feedback, while for larger values of  $\Omega$  the fidelity of the encoded qubit is clearly improved relative to what it would be for a bare qubit.

In conclusion, we have described a novel approach to continuous quantum error correction based on station-

ary coherent feedback. Our scheme may match well with hardware implementations that feature solid-state qubits embedded in planar circuits of electromagnetic resonators and wave-guides, and establishes important new connections between QEC and coherent-feedback quantum control theory. While our current results are limited to the bit/phase-flip scenarios, we hope in future work to find ways to combine bit-flip and phase-flip probe interactions (possibly employing either the five-qubit code [1] or Bacon-Shor subsystem code [24]) to design feedback networks that can correct arbitrary single-qubit errors. We also hope to exploit the capacity of coherent signal fields to carry syndrome information simultaneously in two quadratures to enable more resource-efficient implementations of coherent-feedback QEC.

This work has been supported by IARPA (W911NF-08-1-0491) and by HP Labs. HN acknowledges the support of the Australian Research Council (DP0986615).

- 
- [1] D. Gottesman, arXiv:0904.2557v1 [quant-ph] (2009).
  - [2] S. Das Sarma, M. Freedman and C. Nayak, Phys. Rev. Lett. **94**, 166802 (2005).
  - [3] D. Bacon, Phys. Rev. A **73**, 012340 (2006).
  - [4] L. Jiang *et al.*, Nature Physics **4**, 482 (2008).
  - [5] J. Kerckhoff *et al.*, Phys. Rev. A **79**, 024305 (2009).
  - [6] C. Ahn, A. C. Doherty and A. J. Landahl, Phys. Rev. A **65** 042301 (2002).
  - [7] C. Ahn, H. M. Wiseman and G. J. Milburn, Phys. Rev. A **67** 052310 (2003).
  - [8] M. Sarovar *et al.*, Phys. Rev. A **69**, 052324 (2004).
  - [9] C. Ahn, H. M. Wiseman and K. Jacobs, Phys. Rev. A **70**, 024302 (2004).
  - [10] R. van Handel and H. Mabuchi, arXiv:quant-ph/0511221v1 (2005).
  - [11] O. Oreshkov and T. A. Brun, Phys. Rev. A **76**, 022318 (2007).
  - [12] B. A. Chase, A. J. Landahl and J. M. Geremia, Phys. Rev. A **77**, 032304 (2008).
  - [13] M. R. James, H. I. Nurdin and I. R. Petersen, IEEE Trans. Automat. Contr. **53**, 1787 (2008).
  - [14] H. I. Nurdin, M. R. James and I. R. Petersen, Automatica **45**, pp. 1837-1846 (2009) ; arXiv:0711.2551v2.
  - [15] H. I. Nurdin, M. R. James and A. C. Doherty, to appear in SIAM J. Control Optim. (2009); arXiv:0806.4448v1 [quant-ph].
  - [16] H. Mabuchi, Phys. Rev. A **78**, 032323 (2008).
  - [17] D. Englund *et al.*, Opt. Express **15**, 5550 (2007).
  - [18] P. Majer *et al.*, Nature **449**, 443 (2007).
  - [19] J. Barclay *et al.*, arXiv:0904.0500v1 [quant-ph] (2009).
  - [20] L. Bouten, R. van Handel and A. Silberfarb, J. Functional Analysis **254**, 3123 (2008).
  - [21] J. Gough and M. R. James, to appear in IEEE Trans. Automat. Contr. (2009); arXiv:0707.0048v3 [quant-ph].
  - [22] H. Mabuchi, arXiv:0907.2720v1 [quant-ph] (2009).
  - [23] S. M. Tan, J. Opt. B: Quantum Semiclass. Opt. **1**, 424 (1999).
  - [24] P. Aliferis and A. W. Cross, Phys. Rev. Lett. **98**, 220502 (2007).